International Journal of Heat and Fluid Flow 32 (2011) 365–377

Contents lists available at ScienceDirect

International Journal of Heat and Fluid Flow

journal homepage: www.elsevier.com/locate/ijhff

Transport and deposition of neutral particles in magnetohydrodynamic turbulent channel flows at low magnetic Reynolds numbers

C.D. Dritselis *, I.E. Sarris, D.K. Fidaros [1], N.S. Vlachos

Department of Mechanical Engineering, University of Thessaly, Athens Avenue, 38334 Volos, Greece

ARTICLE INFO

Article history:
Received 10 May 2010
Received in revised form 31 December 2010
Accepted 4 January 2011
Available online 1 February 2011

Keywords:
MHD
Turbulent channel flow
Particle transport
Deposition

ABSTRACT

The effect of Lorentz force on particle transport and deposition is studied by using direct numerical simulation of turbulent channel flow of electrically conducting fluids combined with discrete particle simulation of the trajectories of uncharged, spherical particles. The magnetohydrodynamic equations for fluid flows at low magnetic Reynolds numbers are adopted. The particle motion is determined by the drag, added mass, and pressure gradient forces. Results are obtained for flows with particle ensembles of various densities and diameters in the presence of streamwise, wall-normal or spanwise magnetic fields. It is found that the particle dispersion in the wall-normal and spanwise directions is decreased due to the changes of the underlying fluid turbulence by the Lorentz force, while it is increased in the streamwise direction. The particle accumulation in the near-wall region is diminished in the magnetohydrodynamic flows. In addition, the tendency of small inertia particles to concentrate preferentially in the low-speed streaks near the walls is strengthened with increasing Hartmann number. The particle transport by turbophoretic drift and turbulent diffusion is damped by the magnetic field and, consequently, particle deposition is reduced.

© 2011 Elsevier Inc. All rights reserved.

1. Introduction

Magnetohydrodynamic (MHD) turbulent flows at low magnetic Reynolds numbers occur in many scientific fields and engineering applications (e.g., semiconductor crystal growth, electromagnetic melt stirring, MHD pumps, and liquid–metal cooling blankets for fusion reactors). Constant magnetic fields are often used to control the flow and suppress unwanted fluid motions. In many circumstances, transport of particles is also involved. For example, charged impurities are introduced in fusion plasmas due to the erosion of walls (Smirnov et al., 2007; Krasheninnikov et al., 2010). Recent drag reducing and flow control techniques rely on the release of particles into the flow in order to enhance the electric conductivity of the carrier gas and achieve a better performance by a magnetic field (Braun et al., 2008). Moreover, nonmetallic inclusions are often present in liquid–metals affecting the quality of the final product (Takahashi and Tanigushi, 2003).

A significant advance in the existing knowledge of MHD flows has been achieved by experiments (Lykoudis and Brouillette, 1968; Moresco and Alboussière, 2004) and by direct numerical simulations (DNS) in homogeneous turbulence (Zikanov and Thess, 1998; Kassinos et al., 2006, 2007), in turbulent channel (Lee and Choi, 2001; Boeck et al., 2007; Shatrov and Gerbeth, 2007; Krasnov et al., 2008) or pipe flows (Satake et al., 2002), and in natural convection in cylindrical cavities (Kakarantzas et al., 2009; Sarris et al., 2010) at low magnetic Reynolds numbers. A summary of related studies is provided by Knaepen and Moreau (2008). Despite of their relevance, studies of MHD turbulent flows laden with particles using DNS are limited (Rouson et al., 2008; Homann et al., 2009). In Rouson et al. (2008), a new tensor statistic was proposed to describe the preferred orientation of particle clusters in MHD homogeneous turbulence. The neutral particles exhibited a tendency to concentrate in certain flow regions. Thus, the changes in the homogeneous turbulence by the magnetic field were reflected on the spatial particle distributions and were quantified by using the new tensor statistic.

It is known that due to inertial bias in the particle trajectories, high instantaneous particle concentration is observed in flow regions of low vorticity or high strain-rate (Squires and Eaton, 1991; Eaton and Fessler, 1994; Fessler et al., 1994). It was also shown that the preferential concentration of particles is more pronounced for particles with time constants and settling velocities close to the Kolmogorov scales (Wang and Maxey, 1993). For turbulent channel flows, it is accepted that the near-wall particle concentration is non-uniform in the spanwise direction and the largest particle number density occurs in the low-speed streaks (Pedinotti et al., 1992; Kaftori et al., 1995; Pan and Banerjee, 1996). These

* Corresponding author. Tel.: +30 24210 74075; fax: +30 24210 74085.
E-mail address: dritseli@mie.uth.gr (C.D. Dritselis).
[1] Present address: Centre for Research and Technology-Thessaly, 38500 Volos, Greece.

0142-727X/$ - see front matter © 2011 Elsevier Inc. All rights reserved.
doi:10.1016/j.ijheatfluidflow.2011.01.002

Nomenclature

b^*	characteristic magnetic field, $b^* = \|\mathbf{b}_0^*\|$
$\mathbf{b}_0$	external magnetic field
C_0	initial particle concentration
C_D	drag coefficient
C_{np}	mean particle number density
C_w	drag coefficient due to the wall
D_i	particle dispersion coefficients
d_p	particle diameter
h	half distance between the channel walls
Ha	Hartmann number, $Ha = b^*\delta^*(\sigma/\rho_f\nu)^{1/2}$
J_p	particle mass flux onto the walls
N	Stuart number, $N = \sigma b^{*2}\delta^*/\rho_f U^*$
np_0	initial number of particles
np_d	number of particles deposited
p	instantaneous fluid pressure
PD_{cnp}	probability density function of the conditional particle number density
PD_{Fin}	probability density function of particle flux toward the wall
PD_{Fout}	probability density function of particle flux toward the outer region
PD_{Q2}	probability density function of ejection events
PD_{Q4}	probability density function of sweep events
$Q2$	ejection events
$Q4$	sweep events
Re	Reynolds number, $Re = U^*\delta^*/\nu$
Re_m	magnetic Reynolds number, $Re_m = U^*\delta^*/\nu_m$
Re_p	particle Reynolds number, $Re = \|u^* - v^*\|d_p^*/\nu$
Re_τ	Reynolds number based on the friction velocity, $Re_\tau = u_\tau h/\nu$
$R_{f@p,i}$	autocorrelation of the fluid velocity seen by the particles
$R_{p,i}$	autocorrelation of the particle velocity
S	particle–fluid density ratio, $S = \rho_p/\rho_f$
t	time
t_d^+	time interval
$T_{f@p,i}$	Lagrangian time scale of the fluid velocity seen by the particles
$T_{p,i}$	Lagrangian time scale of the particle velocity
t_R^+	particle residence time
$\mathbf{u}$	instantaneous fluid velocity
U^*	characteristic fluid velocity scale
$\tilde{u}^n_{@p,i}$	locally undisturbed fluid velocity at the particle position
u_b	bulk fluid velocity
u_d^+	non-dimensional deposition velocity
U_i	mean fluid velocity
u_i'	fluid velocity fluctuation
u_τ	wall friction velocity, $u_\tau = (\tau_w/\rho_f)^{1/2}$
V_i	mean particle velocity
v_i'	particle velocity fluctuation
$v_{i,dep}$	particle impinging velocity
v_i^n	velocity of the n particle
x_1, x_2, x_3	streamwise, wall-normal and spanwise coordinates
y_0^+	distance from the channel wall
Y_i^2	mean-square particle displacement
y_i^n	position of the n particle

Greek symbols

δ^*	characteristic length scale
η	distance of the particle centre from the wall
ν	fluid kinematic viscosity
ν_m	magnetic diffusivity
ρ_f	fluid density
ρ_p	particle density
σ	fluid electric conductivity
τ_p	particle response time, $\tau_p = Sd_p^2/18\nu$
τ_w	wall shear stress
φ	electric potential
φ_{diff}	particle flux due to turbulent diffusion
φ_{turbo}	particle flux due to turbuphoretic drift
$\boldsymbol{\omega}$	instantaneous fluid vorticity

Symbols

$\langle\rangle_{Ep}$	quantity averaged over the dispersed phase and the homogeneous planes
$\langle\rangle_{Ef}$	fluid quantity averaged over the homogeneous planes and time
$\langle\rangle_{np;dep}$	quantity conditionally averaged over all depositing particles
$\langle\rangle_{np}$	quantity averaged over np particles
$\langle\rangle_{vol}$	quantity averaged over the volume of the flow domain
$\parallel$	wall-parallel direction
$\perp$	wall-normal direction
$*$	dimensional quantity
$+$	quantity in wall units

non-uniformities of the particle concentration were related to the underlying organized fluid motions (Rouson and Eaton, 2001; Marchioli and Soldati, 2002). In the core region, the particle distribution is not correlated to any coherent structures, although particles are also preferentially concentrated there (Fessler et al., 1994). The latter is believed to be due to convection of the near-wall inhomogeneities of particle concentration into the outer flow.

The present study investigates the magnetic field effect on the transport and deposition of uncharged particles in connection with the modifications of the fluid flow structures. It is known that simple vortices are mostly enlarged in the direction of the applied magnetic field (Davidson, 1997; Davidson, 1999). For homogeneous MHD turbulent flow, the vortical events are similarly elongated in the direction of the external magnetic field, with a smaller enlargement in the transverse directions (Zikanov and Thess, 1998; Kassinos et al., 2006; Kassinos et al., 2007). In MHD turbulent channel flow, an increase in the size of vortical structures was observed by Lee and Choi (2001) and Krasnov et al. (2008). To our best knowledge, this is the first attempt to study several aspects of particle-laden MHD turbulent channel flow. This study contributes to a better understanding of how particle transport and deposition are affected by the changes of the fluid flow due to the magnetic field. Except of their theoretical value, the results are also of practical interest, since they can potentially help the development of efficient techniques capable of separating neutral particles from electrically conducting fluids.

2. Governing equations

The equations of turbulent flow of an incompressible and electrically conducting fluid at low magnetic Reynolds numbers ($Re_m \ll 1$) in non-dimensional form are

$$\nabla \cdot \mathbf{u} = 0, \tag{1}$$

$$\frac{\partial \mathbf{u}}{\partial t} + (\mathbf{u}\cdot\nabla)\mathbf{u} = -\nabla p + Re^{-1}\nabla^2\mathbf{u} + N[(-\nabla\varphi + \mathbf{u}\times\mathbf{b}_0)\times\mathbf{b}_0], \tag{2}$$

$$\nabla^2\varphi = \nabla(\mathbf{u}\times\mathbf{b}_0) = \mathbf{b}_0\cdot\boldsymbol{\omega}, \tag{3}$$

where $\mathbf{u}$, p, and $\boldsymbol{\omega}$ are the fluid velocity, pressure, and vorticity, respectively, φ is the electric potential, $\mathbf{b}_0$ is the uniform magnetic field, and bold symbols indicate vectors. The non-dimensional velocity, space, and time are defined as $\boldsymbol{u} = \boldsymbol{u}^*/U^*$, $\boldsymbol{x} = \boldsymbol{x}^*/\delta^*$, and $t = t^*U^*/\delta^*$, respectively, where $*$ indicates dimensional quantities, and U^*, δ^* are proper characteristic velocity and length scales, respectively. The non-dimensional pressure is $p = p^*/\rho_f U^{*2}$, where ρ_f is the fluid density. The non-dimensional magnetic field and electric potential are $\mathbf{b}_0 = \mathbf{b}_0^*/b^*$ and $\varphi = \varphi^*\delta^*/U^*b^*$, respectively, where $b^* = |\mathbf{b}_0^*|$ is a characteristic quantity so that $\mathbf{b}_0$ is a unit vector. $Re(=U^*\delta^*/\nu)$ and $N(=\sigma b^{*2}\delta^*/\rho_f U^*)$ are the Reynolds and Stuart (interaction parameter) numbers, respectively, which are related to the Hartmann number Ha through $N = Ha^2/Re$, where ν and σ are the kinematic viscosity and electric conductivity of the fluid, respectively. Periodic boundary conditions are applied in the streamwise (x_1) and spanwise (x_3) directions, and no-slip conditions at the non-conducting walls (i.e., $\partial\varphi/\partial x_2 = 0$). For the cases with a wall-normal magnetic field, the open circuit condition is also adopted (Lee and Choi, 2001).

The position y_i^n and the velocity v_i^n of the n particle are determined in a Lagrangian frame by

$$\frac{dy_i^n}{dt} = v_i^n, \tag{4}$$

$$\frac{dv_i^n}{dt} = \frac{3}{4}\frac{\rho_f}{\rho_p}\frac{C_D C_w}{d_p}|\tilde{\mathbf{u}}_{@p}^n - \mathbf{v}^{\mathbf{n}}|(\tilde{u}_{@p,i}^n - v_i^n) + \frac{1}{\rho_f}\frac{D\tilde{u}_{@p,i}^n}{Dt} + \frac{1}{2\rho_f}\left(\frac{D\tilde{u}_{@p,i}^n}{Dt} - \frac{dv_i^n}{dt}\right), \tag{5}$$

where $\tilde{u}_{@p,i}^n$ is the locally undisturbed fluid velocity at the particle position, and ρ_p, d_p are the particle density and diameter, respectively. Eqs. (4) and (5) are made non-dimensional by using the same characteristic scales as for the fluid flow. The right hand side terms of Eq. (5) are the drag, the pressure gradient, and the added mass forces, respectively. Gravity is not considered in order to concentrate on the effects of the MHD turbulence on the trajectories of uncharged, non-colliding particles. The Stokes drag force is corrected by the coefficient C_D given by

$$C_D = \frac{24}{Re_p}(1 + 0.15Re_p^{0.687}). \tag{6}$$

to account for inertial effects at non-negligible particle Reynolds numbers

$$Re_p = |\tilde{\mathbf{u}}^{*n} - \mathbf{v}^{*n}|d_p^*/\nu(= |\tilde{\mathbf{u}}^n - \mathbf{v}^{\mathbf{n}}|d_p Re),$$

The increase of the drag force due to the channel walls is accounted for by multiplying the drag force with the coefficient C_w, given as (Pan and Banerjee, 1996)

$$C_{w,\parallel} = \left[1 - \frac{9}{32}\frac{d_p}{\eta} + \frac{1}{64}\left(\frac{d_p}{\eta}\right)^3\right]^{-1} + O\left[\left(\frac{d_p}{\eta}\right)^5\right], \tag{7}$$

$$C_{w,\perp} = \left[1 - \frac{9}{16}\frac{d_p}{\eta} + \frac{1}{16}\left(\frac{d_p}{\eta}\right)^3\right]^{-1} + O\left[\left(\frac{d_p}{\eta}\right)^5\right], \tag{8}$$

where η is the distance of the particle centre from the wall, and the symbols $\parallel$ and $\perp$ indicate components in the wall-parallel and wall-normal directions, respectively.

Eq. (5) is appropriate for particles with diameters of the same order or smaller than the smallest length scales of the fluid flow. It has also been used for the numerical study of the particle dynamics in turbulent open channel flows (Pan and Banerjee, 1996) with particle diameters and phase density ratios similar to the present study. It has been shown that a particle immersed in an electrically conducting fluid experiences a rigid body motion by the combined action of the electric and magnetic fields (Leenov and Kolin, 1954; Moffatt and Sellier, 2002; Sellier, 2003). For particles with small diameter, such short range perturbations are probably dissipated by the viscous action and they are not considered here. The Basset and Saffmann lift forces have been neglected in Eq. (5) in order to restrict the range of parameters studied. The Saffmann lift force can increase particle deposition, but its importance over the drag force is significantly reduced by applying proper corrections for turbulent channel flow (Wang et al., 1997). The Basset force is significant across the whole spectrum from light-to-heavy particles, but its treatment is computationally involved and it is usually discarded (Armenio and Fiorotto, 2001).

Particle–particle collisions and particle feedback effects are not considered in this one-way coupling treatment. Thus, the validity of the present results is limited to mixtures with low particle volume fractions. The locally undisturbed fluid velocity at the particle position $\tilde{u}_{@p,i}^n$ is approximated from the velocity obtained by the solution of Eqs. (1)–(3). Particles exiting the domain in the streamwise and spanwise directions are reintroduced in it by using periodic conditions, while elastic particle–wall collisions are considered. However, for the study of particle deposition, perfectly absorbing walls are considered, consistent with previous numerical studies (McLaughlin, 1989; Wang et al., 1997; Zhang and Ahmadi, 2000). When a particle hits one wall for the first time, it is labelled as a deposited particle, while its trajectory calculation is continued and the particle may enter the central flow region or hit the walls again. In the latter case, the next collisions of the labelled particle with the walls are not considered in the calculation of the particle deposition rates. Geometric criteria are used to identify the deposition of particles, e.g., when their centre is less than $d_p/2$ distance from the solid boundary.

3. Numerical methods and solution procedure

The numerical algorithm used to solve Eqs. (1)–(3) is based on a semi-implicit, fractional step method. The time integration incorporates an implicit second-order Crank–Nicolson method for the diffusion terms and an explicit second-order Adams–Bashforth method for the convection terms and the Lorentz force. All spatial derivates are discretized with a second-order central differencing scheme. Poisson equations are solved for the pseudo-pressure and the electric potential by FFT in the periodic directions and tri-diagonal matrix inversion in the wall-normal direction (Orlandi, 2000). The trajectory of each particle is computed simultaneously with the fluid flow field by solving Eqs. (4) and (5) with a second-order Adams–Bashforth method. The fluid velocity at the particle position is calculated by interpolation with fifth-order Lagrange polynomials.

Direct numerical simulations are performed at a Reynolds number of 4000 based on the bulk velocity u_b and the channel width $2h$. This corresponds to $Re_{\tau,0} \approx 135$ based on the wall friction velocity $u_{\tau,0} = (\tau_{w,0}/\rho_f)^{1/2}$ and h, where $\tau_{w,0}$ is the wall shear stress and the subscript '$_0$' indicates quantities of the hydrodynamic case. The dimensions of the channel are $3\pi h \times 2h \times \pi h$ in the x_1, x_2, and x_3-directions, respectively. For all cases, the computational grid is $64 \times 97 \times 96$ in the streamwise, wall-normal, and spanwise directions, respectively. The grid spacing is uniform in the periodic directions and uneven in the x_2-direction based on a hyperbolic tangent function. The Stuart and Hartmann numbers examined are: $N_1 = 0.1$, 0.2 and $Ha_1 = 20$, 28.3 for a streamwise magnetic field, $N_2 = 0.006$, 0.01 and $Ha_2 = 4.9$, 6.3 for a wall-normal magnetic field, and $N_3 = 0.01$, 0.025 and $Ha_3 = 6.3$, 10 for a spanwise

magnetic field. The index i of N and Ha indicates the direction of the external magnetic field. For comparison purposes, the size of the channel, the computational mesh, and the values of Re and N used here are the same as those used by Lee and Choi (2001). The values of N covered here are limited to those for which no transition to the laminar regime was found by Lee and Choi (2001).

Two types of numerical experiments were carried out: In the first, the objective was to characterise the inhomogeneity of the Lagrangian statistics describing particle dispersion. For this reason, 10,000 particles with $d_p^* = 10$ μm and $S = \rho_p/\rho_f = 250$ were distributed in each of 48 x_1–x_3 planes from the wall to the channel centreplane and tracked, for several cases without and with magnetic field. For each particle set, the mean-square displacement, the particle dispersion coefficients, and the time scales of the fluid velocity along the particle trajectory were calculated. Further increase of the number of particles revealed only small differences in the Lagrangian statistics (see also, Rambaud et al., 2002) and, thus, groups of 10,000 particles were used to generate these results.

In the second type of simulations, the interest was focused on assessing the magnetic field effect on the particle preferential concentration and deposition rates. A total number of 250,000 particles were uniformly distributed inside the flow domain, which is considered sufficient to provide accurate particle statistics in the same manner as for the fluid flow (Marchioli and Soldati, 2002; Marchioli et al., 2007). After an initial transient, the particulate phase reaches a stationary state, where the mean statistics do not significantly change with time. Thus, the results from these simulations are independent of the initialisation of the particles. The particle–fluid density ratios were $S = 2.5$, 25, and 250 to account for situations corresponding to impurities in liquid–metals and in less conducting fluids (e.g., salt water), or to a weakly ionized gas. The particle diameters were $d_p^* = 100$ μm, 30 μm, and 10 μm, respectively, and the particle response time was $\tau_p^+ = \tau_p^* u_\tau^2/\nu = 1$ with $\tau_p^* = S d_p^{*2}/18\,\nu$. The superscript '+' denotes quantities made non-dimensional in wall units. The effect of particle inertia was also examined by keeping constant the particle diameter at $d_p^* = 30$ μm and increasing the phase density ratio S. The dimensionless response times studied were $\tau_p^+ = 1$, 10, 25, and 100 for $S = 25$, 250, 625, and 2500, respectively. For both types of simulations, the initial particle velocities were equal to those of the fluid at the particle positions for either fully developed hydrodynamic or MHD flows.

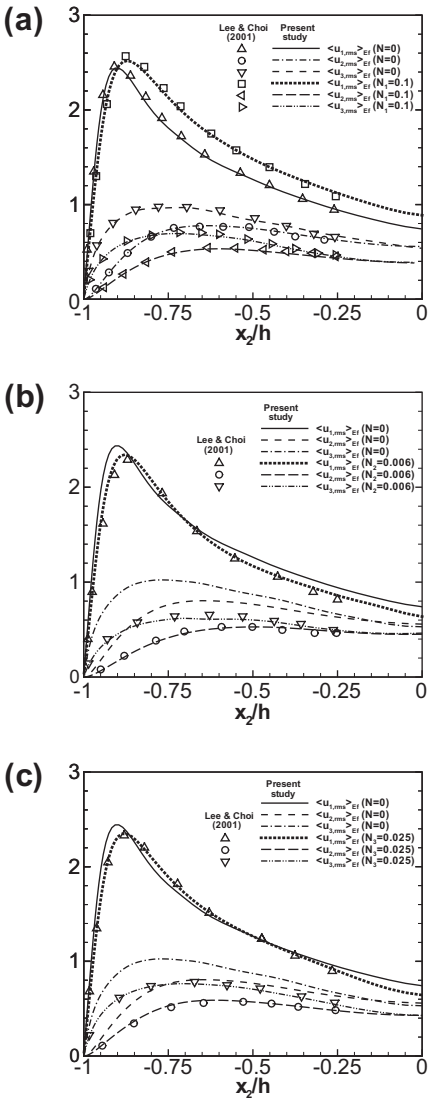

Fig. 1. Distributions of the rms fluid velocity fluctuations normalized by the wall friction velocity with (a) streamwise ($N_1 = 0.1$), (b) wall-normal ($N_2 = 0.006$), and (c) spanwise ($N_3 = 0.025$) magnetic fields.

4. Results and discussion

4.1. Mean and rms fluid velocities

Fig. 1 shows the root-mean-square (rms) of the fluid velocity fluctuations $\langle u_{i,rms}^+ \rangle_{Ef}$ normalized by the wall friction velocity for several cases without ($N = 0$) and with magnetic field in the streamwise ($N_1 = 0.1$), wall-normal ($N_2 = 0.006$), or spanwise ($N_3 = 0.025$) direction. Here, $\langle\rangle_{Ef}$ indicates quantities of the fluid flow averaged over time and the homogeneous directions. Fig. 1 shows a good agreement of the present predictions of $\langle u_{i,rms}^+ \rangle_{Ef}$ with the results of Lee and Choi (2001). The mean streamwise fluid velocity $\langle U_1^+ \rangle_{Ef}$ normalized by the wall friction velocity for the aforementioned cases is shown in Fig. 2. Upward shifts of $\langle U_1^+ \rangle_{Ef}$ in the central region are observed in all the MHD flows. For the case of the wall-normal magnetic field, this is due to the small value of the Stuart number studied. Qualitatively similar results have been found both experimentally and numerically (Lykoudis and Brouillette, 1968; Sarris et al., 2007; Krasnov et al., 2008).

The two components of $\langle u_{i,rms}^+ \rangle_{Ef}$ in the directions perpendicular to the magnetic field are directly damped by the Lorentz force, whereas that in the parallel direction is indirectly affected (Lee and Choi, 2001; Dritselis and Vlachos, 2009). The indirect changes relate possibly to the suppression by the magnetic field of the pressure fluctuations and the spatial gradients of the fluid velocities.

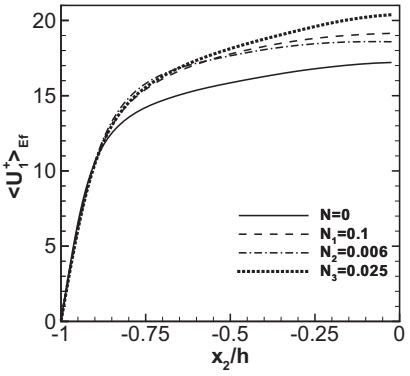

Fig. 2. Distribution of the mean streamwise fluid velocity normalized by the wall friction velocity without magnetic field ($N = 0$) and with streamwise ($N_1 = 0$), wall-normal ($N_2 = 0.006$), and spanwise ($N_3 = 0.025$) magnetic fields.

This influences the inter-component energy exchange, resulting in a reduction of the cross-flow velocity fluctuations and the '*bottle up*' of the streamwise ones. The latter fluctuations can also be enhanced for a streamwise magnetic field due to the absence of any direct damping effect in the x_1-direction. A wall-normal magnetic field can alter the mean and the turbulent flow affecting the production of fluid turbulence and, thus, producing indirect changes in the fluid velocity fluctuations.

4.2. Particle transport

4.2.1. Particle dispersion from plane sources

Results are presented addressing the effect of the magnetic field on the dispersion of particles initially released from plane sources. For all cases, the particle dispersion exhibited qualitatively similar trends to fluid particle diffusion (Taylor, 1921; Choi et al., 2004; Luo et al., 2007). The square of particle displacement (dispersion) is initially proportional to the square of time, while the later-time dispersion is proportional to time. However, the particle dispersion in the streamwise direction is mostly affected by the mean flow and to a lesser extent by the mean shear. Moreover, the wall-normal particle dispersion is influenced by the limited distance a particle can travel in the x_2-direction. Fig. 3 shows the dispersion coefficients D_i for each particle group as a function of their initial locations in the normal direction at time t_0, defined as

$$D_i(t) = \frac{1}{2}\frac{dY_i^2}{dt}, \tag{9}$$

where the mean-square displacement Y_i^2 in the i-direction of a group of np particles is calculated as

$$Y_i^2 = \frac{1}{np}\sum_{n=1}^{np}[y_i^n(t) - y_i^n(t_0)]^2. \tag{10}$$

We focused on the long-term behaviour in which the linear part of Y_i^2 was established. For all cases, D_i was calculated in the time interval between $t^+ = 455$ and $t^+ = 610$ after the release of particles, which is long enough for an accurate assessment of the long-time variation of Y_i^2 (Rambaud et al., 2002; Choi et al., 2004). An overall behaviour of the changes in the fluid flow by the magnetic field is illustrated in Fig. 4, showing the time histories of the volume averaged fluid velocity variances $\langle u_i^2\rangle_{vol}$. The trends of the curves in Fig. 4 are consistent with the distributions of $\langle u_{i,rms}^+\rangle_{Ef}$ shown in Fig. 1.

The inhomogeneity of D_i is apparent in Fig. 3 for both the hydrodynamic and MHD flows. The distributions of D_1 and D_3 are quite similar and increase asymptotically with increasing distance from the wall. In contrast, the largest value of D_2 is observed close to the wall and it is gradually reduced toward the centre-plane. In the MHD cases, D_1 is increased in the outer flow region, while D_2 and D_3 are reduced throughout the channel. It is seen that the magnetic field effect on D_i is anisotropic; the disparity between the streamwise and the cross-flow components of D_i is increased, which is more pronounced for a wall-normal magnetic field. Two of the parameters influencing the long-term particle dispersion, and consequently D_i, are the mean and rms particle velocities. In this study, the changes in D_i by the magnetic field can be explained by observing the corresponding fluid turbulence suppression. This is because, for non-colliding particles with $\tau_p^+ = 1$, the Eulerian particle statistics (e.g., mean streamwise and rms velocities) coincide with those of the fluid, which was also observed in McLaughlin (1989), Young and Leeming (1997), and Marchioli et al. (2007). The dispersion of such particles is very close to the

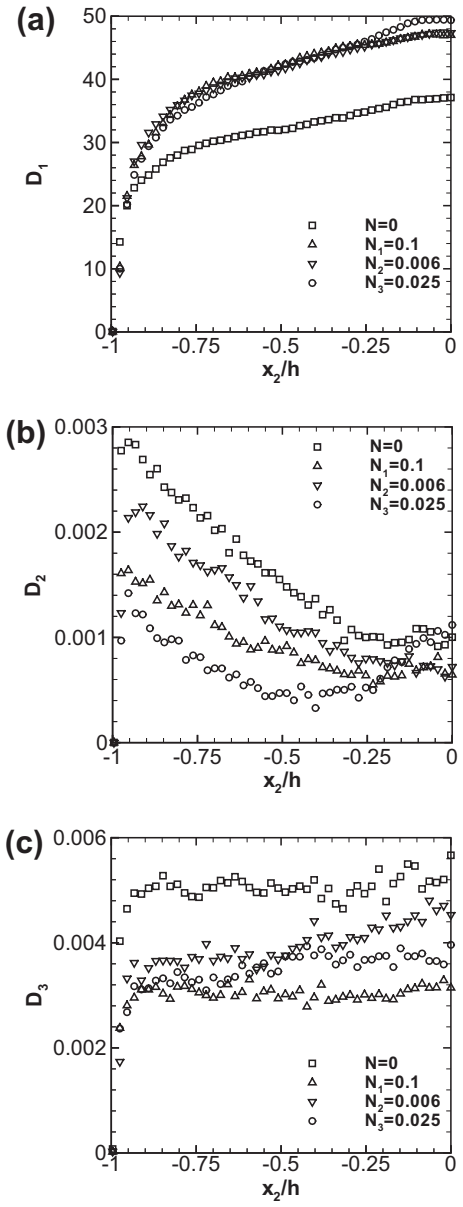

Fig. 3. Distributions of particle dispersion coefficients in the streamwise D_1 (a), wall-normal D_2 (b) and spanwise D_3 (c) directions, without magnetic field ($N = 0$) and with streamwise ($N_1 = 0.1$), wall-normal ($N_2 = 0.006$), and spanwise ($N_3 = 0.025$) magnetic fields.

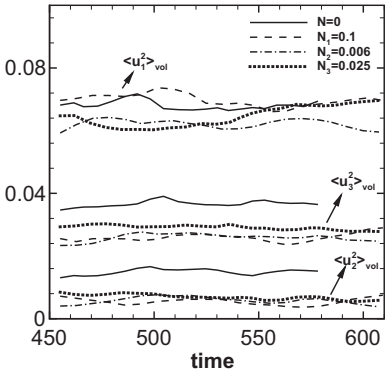

Fig. 4. Time histories of the volume averaged variances of the fluid velocity fluctuations $\langle u_i^2\rangle_{vol}$ for the cases without magnetic field ($N = 0$) and with streamwise ($N_1 = 0.1$), wall-normal ($N_2 = 0.006$) and spanwise ($N_3 = 0.025$) magnetic fields. The values of $\langle u_2^2\rangle_{vol}$ are shifted downwards by 0.015.

diffusion of fluid tracers and, thus, the changes in the fluid flow are reflected on their motion.

In particular, the wall-normal and spanwise fluid velocity fluctuations are reduced with increasing N. This is observed in Fig. 1 for all wall-normal positions, independent of the orientation of the magnetic field. Particle dispersion in these directions is decreased and, consequently, D_2 and D_3 are reduced. On the other hand, the streamwise particle dispersion is influenced by both the mean flow and the turbulent fluctuations. Fig. 2 shows that, in the presence of a streamwise or spanwise magnetic field, the mean streamwise fluid velocity is decreased near the walls and it is increased in the rest of the flow region. In addition, Fig. 1 shows that the streamwise fluid velocity fluctuations are increased away from the wall for a streamwise magnetic field. These changes are also observed in the corresponding Eulerian and Lagrangian statistics of the particles with $\tau_p^+ = 1$. Thus, the mean-square displacement in the streamwise direction is increased, resulting in the augmentation of D_1. The same applies for a wall-normal magnetic field, which also modifies directly the mean velocity leading to the changes of D_1 shown in Fig. 3.

For each particle set, the Lagrangian autocorrelation of the fluid velocity "seen" by the particles was computed:

$$R_{f@p,i}[t; y_2^n(t_0)] = \frac{\langle u'_{@p,i}[t_0; y_2^n(t_0)] u'_{@p,i}[t+t_0; y_2^n(t_0)]\rangle_{np}}{\langle u'^2_{@p,i}[t_0; y_2^n(t_0)]\rangle_{np}^{1/2} \langle u'^2_{@p,i}[t+t_0; y_2^n(t_0)]\rangle_{np}^{1/2}}, \qquad (11)$$

where $\langle\rangle_{np}$ indicates averaging over the np particles of each group, the prime denotes fluctuation about the mean, and the repeated index does not imply summation. All the averaged quantities in Eq. (11) are functions of the time difference t. The term after the semicolon in Eq. (11) indicates the group of particles, identified by their initial wall-normal position $y_2^n(t_0)$, for which these quantities are calculated. This is done in order to assess the effect of flow inhomogeneity on the Lagrangian statistics. Fig. 5 shows the distributions of the associated Lagrangian time scale $T_{f@p,i}$. Similarly to previous studies (Rambaud et al., 2002; Luo et al., 2007), $T_{f@p,i}$ was estimated as the time when the autocorrelation crosses the threshold value of e^{-1}, instead of integrating Eq. (11) over time. $T_{f@p,i}$ can be regarded as a rough measure of the time interval over which the fluid velocity along the particle trajectory is correlated with itself. Fig. 5 shows that $T_{f@p,1}$ is generally larger than $T_{f@p,2}$ and $T_{f@p,3}$. The particles respond to the changes in the underlying fluid motions by the magnetic field, "seeing" a turbulence that is correlated over longer times and, thus, the time scales are increased.

The Lagrangian time scale of the fluid velocity along the particle trajectory in the streamwise direction is longer than those in the other two directions. This can be attributed to the interaction of particles with the flow coherent structures. Inertial particles are thrown out from intense vortical regions concentrating in regions of low streamwise fluid velocity (Pedinotti et al., 1992; Eaton and Fessler, 1994; Kaftori et al., 1995). Eventually, the particles see lower streamwise fluid velocities, which are autocorrelated over longer times relative to the other components, the situation being similar in the MHD cases. The increase of $T_{f@p,1}$ is an indirect evidence of the increased size of the structures in the streamwise direction by the magnetic field. A similar but smaller enlargement of the turbulent structures in the wall-normal and spanwise directions is also indicated by the increased values of $T_{f@p,2}$ and $T_{f@p,3}$, respectively. The changes in $T_{f@p,i}$ reveal that the near-wall turbulent structures are more effectively modified by a wall-normal magnetic field. Fig. 5 shows a small effect of the spanwise magnetic field on $T_{f@p,i}$, especially in the central flow region. This is related to the corresponding smaller changes in the turbulent structures, which consist of their enlargement mainly in the streamwise direction, due to the mean shear, and to a lesser extent in the other two directions (Lee and Choi, 2001; Krasnov et al., 2008; Dritselis and Vlachos, 2009).

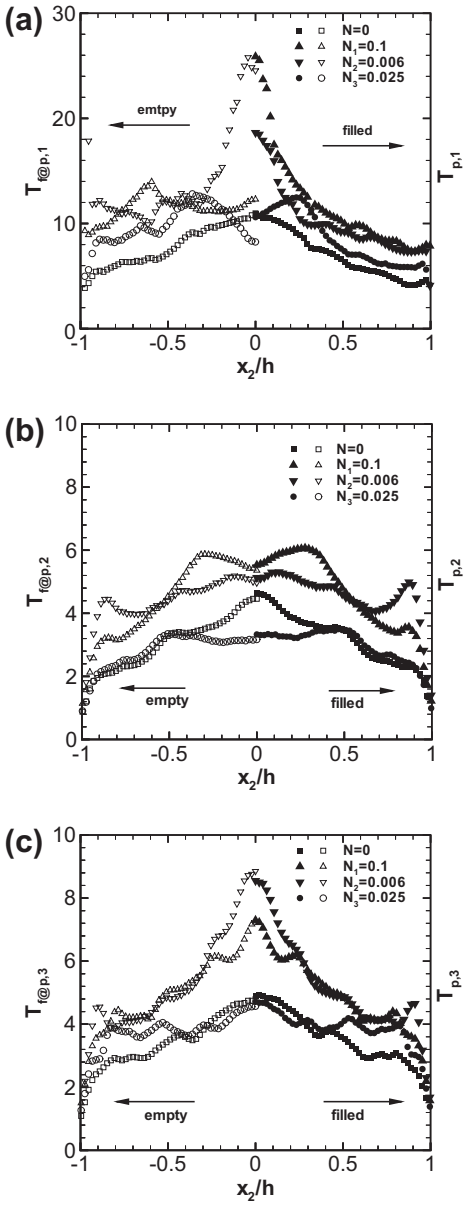

Fig. 5. Distributions of the Lagrangian time scales of the particle velocity $T_{p,i}$ (filled symbols) and of the velocity seen by the particles $T_{f@p,i}$ (empty symbols) in the streamwise $T_{p,1}$, $T_{f@p,1}$ (a), wall-normal $T_{p,2}$, $T_{f@p,2}$ (b) and spanwise $T_{p,3}$, $T_{f@p,3}$ (c) directions, without magnetic field ($N = 0$) and with streamwise ($N_1 = 0.1$), wall-normal ($N_2 = 0.006$), and spanwise ($N_3 = 0.025$) magnetic fields.

In order to explain the effect of the magnetic field orientation on D_i, the Lagrangian time scales associated with the particle velocities $T_{p,i}$ are required. The particle velocity autocorrelations $R_{p,i}$ and $T_{p,i}$ were calculated in the same manner as $R_{f@p,i}$ and $T_{f@p,i}$ using the velocity fluctuations of the particles instead of the fluid in Eq. (11). The distributions of $T_{p,i}$ are shown in Fig. 5, revealing subtle differences as compared to those of $T_{f@p,i}$ due to the small inertia of the particles studied. Thus, similar inferences to those for $T_{f@p,i}$ can be formulated also for $T_{p,i}$. The changes in D_i with respect to the orientation of the magnetic field can be explained based on Figs. 1, 2, 4 and 5. In particular, D_1 seems to be affected mostly by the mean streamwise velocity indicating a dependence on the square value of $\langle U_1\rangle_{Ef}$ (Choi et al., 2004; Luo et al., 2007). The increase of $\langle U_1\rangle_{Ef}$ in the larger part of the channel, due to the magnetic field, leads

to a corresponding increase of D_1. Moreover, the small differences in $\langle U_1\rangle_{Ef}$ for the MHD cases result also in small changes in D_1. The relatively larger (smaller) values of D_1 observed at $x_2/h > -0.5$ ($x_2/h < -0.5$) for $N_3 = 0.025$ as compared to those for $N_1 = 0.1$ and $N_2 = 0.006$ are also consistent with the trends in the corresponding distributions of $\langle U_1\rangle_{Ef}$.

The long-term particle dispersion in the wall-normal and spanwise directions depends on the corresponding variances of the velocity fluctuations and the associated Lagrangian time scales. Due to the wall constraint, the particles are dispersed uniformly in the channel after sufficient time and the volume averaged fluid velocity variances shown in Fig. 4 are proper measures of the velocity fluctuations. The competing changes in these variances and the Lagrangian time scales by the magnetic field seem to control the decrease of D_2 and D_3 with respect to the hydrodynamic case. The overall reduction of D_2 and D_3 in all the MHD cases indicates that the suppression of the velocity fluctuations has a more significant impact on the particle dispersion than the increase of the relevant Lagrangian time scales.

Figs. 4 and 5 indicate that the smallest $\langle u_2^2\rangle_{vol}$ and $\langle u_3^2\rangle_{vol}$ and the largest associated Lagrangian time scales for most of the flow are observed for a wall-normal magnetic field. This combination is responsible for the small effect of the wall-normal magnetic field on the distributions of D_2 and D_3. Fig. 4 indicates also approximately the same values of $\langle u_2^2\rangle_{vol}$ in the cases with $N_1 = 0.1$ and $N_3 = 0.025$. However, the Lagrangian time scale in the x_2-direction is larger for the streamwise magnetic field as shown in Fig. 5. Consequently, smaller values of D_2 are observed for a spanwise than a streamwise magnetic field. The variations of the velocity fluctuations and of $T_{p,2}$ ($T_{f@p,2}$) in the central region result in almost the same values of D_2 for all the MHD cases, revealing a smaller effect of the magnetic field in that region. Fig. 4 shows also sufficiently larger values of $\langle u_3^2\rangle_{vol}$ for the case of $N_3 = 0.025$ as compared to those of $N_1 = 0.1$, while the Lagrangian time scale in the x_3-direction for $N_3 = 0.025$ is little affected. This leads to the smaller reduction of D_3 for the spanwise magnetic field in relation to the streamwise, as illustrated in Fig. 3.

It should be noted that averaging over an ensemble of independent realizations of the particle-laden turbulent flow is generally required for unbiased, stationary statistics (Choi et al., 2004; Luo et al., 2007), which is beyond the scope of the present study. Instead, one realization of a relatively large number of particle trajectories was used for each case (see, Rambaud et al., 2002).

4.2.2. Particle concentration and transfer mechanisms

For all cases, the particles moving toward the central region see higher fluid velocities increasing their own and, thus, they move longer distances. On the other hand, the particles approaching the wall gradually see lower fluid velocities and their velocities are decreased. These particles move shorter distances in the near-wall region, where they remain for longer times, and their dispersion in the wall-normal direction is attenuated. This results in a non-uniform distribution of the mean particle concentration with its maximum value observed near the wall.

Fig. 6 shows the distribution of the mean particle number density C_{np} with distance from the wall. Figs. 6a–c correspond to simulations for three particle sets with $\tau_p^+ = 1$ and $S = 2.5$, 25, and 250, respectively, without magnetic field ($N = 0$) and with a streamwise ($N_1 = 0.1$), wall-normal ($N_2 = 0.006$) or spanwise ($N_3 = 0.025$) magnetic field. The profiles are calculated, firstly, by distributing 96 wall-parallel bins in the x_2-direction unevenly as the computational grid points, of 0.3 wall unit thickness each, and secondly, by counting the fraction of particles inside each bin. In order to account for a larger number of particles in the calculation of C_{np}, averaging over 50 instantaneous realizations of the particle distribution in the time period between $t^+ = 15{,}190$ and $t^+ = 18{,}225$ was performed.

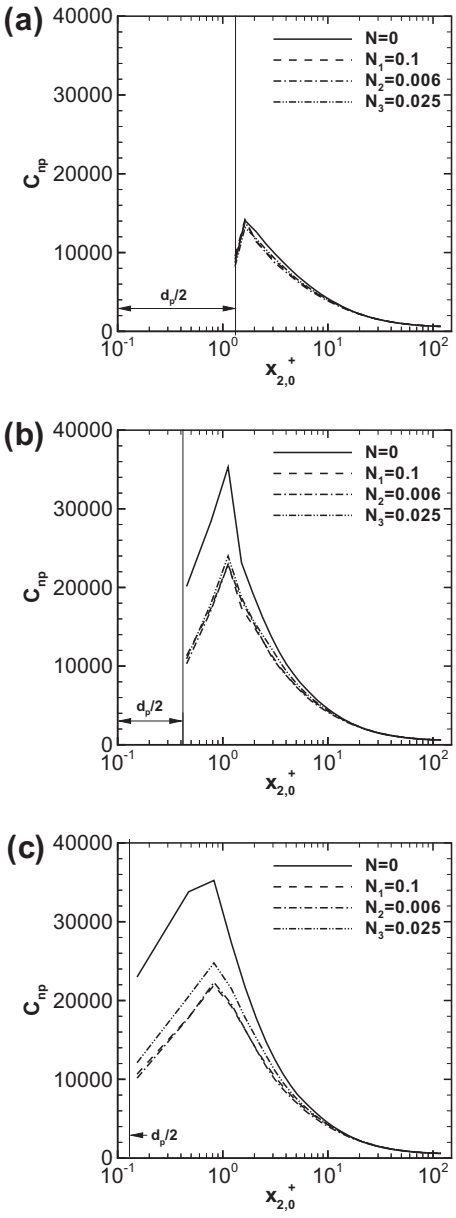

Fig. 6. Distribution of the particle number density for several cases with particles of $\tau_p^+ = 1$ and $S = 2.5$ (a), $S = 25$ (b), and $S = 250$ (c), without magnetic field ($N = 0$) and with streamwise ($N_1 = 0.1$), wall-normal ($N_2 = 0.006$), and spanwise ($N_3 = 0.025$) magnetic fields.

The starting point (smallest $x_{2,0}^+$ value) of the distributions in Fig. 6 is different, since the particles with density ratios of $S = 2.5$, 25, and 250 hit the wall at $x_{2,0}^+ = d_p^+/2 = 1.34$, 0.42, and 0.13, respectively. The inhomogeneity of C_{np} is apparent in Fig. 6 showing high levels of non-uniformities for $x_{2,0}^+ < 20$ independent of the magnetic field. For particles with $S = 25$ and 250, the local maximum value of C_{np} is observed for $x_{2,0}^+ \approx 1$, while C_{np} is decreased as the wall is approached, consistent with the findings of previous studies (McLaughlin, 1989; Marchioli et al., 2007). For the lighter particles of $S = 2.5$, the same behaviour is observed, but the maximum value of C_{np} is located at $x_{2,0}^+ \approx 1.6$. It is evident that the accumulation of particles in the near-wall region is inhibited by the magnetic field. Fig. 6 indicates that, in the MHD flows, the particles are more slowly transferred by the underlying fluid motions from

the core region to the walls decreasing the particle number density for $x^+_{2,0} < 10$. This reduction is more obvious in the cases with particles of $S = 250$ and 25.

Minor changes were observed in the C_{np} distributions by averaging over longer times. The number densities of particles indicate that they are more efficiently transferred toward the wall than away from it during the development period. Statistically steady conditions are gradually achieved for the particle transfer fluxes toward the wall and the outer flow, resulting in the highly non-uniform C_{np} profiles. This phenomenon of particle migration to the walls in turbulent channel flow has been previously recognized (Caporaloni et al., 1975; Reeks, 1983). It is usually attributed to the turbophoretic convective drift of inertial particles in flow regions of low fluid turbulence due to the inhomogeneous velocity fluctuations because of the wall presence. From a statistical point of view, there is a strong possibility for the particles to acquire a motion towards the walls, as an outcome of the inhomogeneity of the moments of the fluid turbulence. Due to their inertia, the particles do not acquire sufficient momentum to escape the near-wall region, resulting in increased local concentrations. The particle concentration profiles in Fig. 6 may be considered to be a consequence of the effects of turbophoretic drift and turbulent diffusion. The turbophoretic drift is responsible for the transport of particles toward the walls and the associated particle flux is $\varphi_{turbo} = -(\rho_p \pi d_p^3/6) C_{np} \tau_p \partial \langle v'_2 \, v'_2 \rangle_{Ep} / \partial x_2$ (Simonin et al., 1993; Young and Leeming, 1997), where $\langle\rangle_{Ep}$ denotes averaging over the dispersed phase and the planes in the homogeneous directions. Turbulent diffusion has a counteracting effect and tends to smooth any spatial gradient of the particle concentration. The diffusive particle flux is defined in Simonin et al. (1993) and Young and Leeming (1997) as $\varphi_{diff} = \langle u_{@p,2} \rangle_{Ep} C_{np} (\rho_p \pi d_p^3/6)$.

Fig. 7 shows the distributions of φ_{turbo} and φ_{diff} for representative particle-laden cases. Negative values of φ_{turbo} are observed near the wall and the opposite is true for φ_{diff}, while a balance between φ_{turbo} and φ_{diff} is approximately achieved. In addition, both $|\varphi_{turbo}|$ and φ_{diff} are reduced by the magnetic field about the same amount. For particles with small inertia, the wall-normal particle velocity correlation $\langle v'_2 \, v'_2 \rangle_{Ep}$ is well approximated by its fluid counterpart $\langle u'_2 \, u'_2 \rangle_{Ef}$ (Young and Leeming, 1997), which is reduced in the MHD flows. Consequently, the total fraction of particles capable of reaching the viscous sublayer is affected. Similarly, the diffusive particle flux is adjusted in order to balance the effect of turbophoresis; it is decreased near the wall due to the reduced local particle concentration. Thus, both mechanisms of turbulent diffusion and turbophoretic drift are significantly attenuated by the magnetic field.

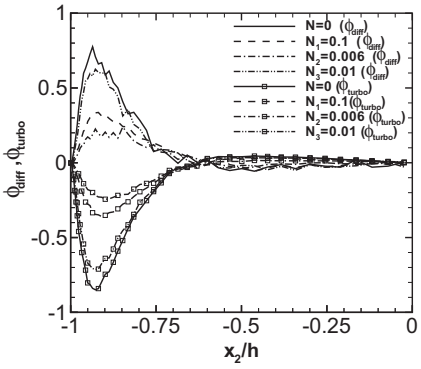

Fig. 7. Distributions of the particle fluxes due to turbophoretic drift φ_{turbo} and turbulent diffusion φ_{diff} for representative particle-laden cases with $S = 250$ and $\tau^+_p = 1$, without magnetic field ($N = 0$) and with streamwise ($N_1 = 0.1$), wall-normal ($N_2 = 0.006$), and spanwise ($N_3 = 0.01$) magnetic fields.

The near-wall turbulent structures create outward motions of low momentum fluid ($Q2$-ejections, $u'_1 < 0$ and $u'_2 > 0$) and inward motions of high-speed fluid ($Q4$-sweeps, $u'_1 > 0$ and $u'_2 > 0$), contributing to the production of fluid turbulence (Kim et al., 1987). In addition, these organized fluid motions provide certain paths through which the particles can approach or move away from the wall, influencing their accumulation in the viscous sublayer. To gain insight into the magnetic field effect on the organized fluid motions in the near-wall region, the probability density functions of ejection (PD_{Q2}) and sweep (PD_{Q4}) events in a region of $5 \leqslant x^+_{2,0} \leqslant 15$ were calculated. Fig. 8a shows the variations of PD_{Q2} and PD_{Q4} with the local wall shear stress τ_w normalized by its mean value $\langle \tau_w \rangle_{Ef}$ for representative cases. It is seen that, for the hydrodynamic flow, the sweep and ejection events are clearly separated around the value of $\tau_w / \langle \tau_w \rangle_{Ef} = 1$. This means that strong ejection events correspond to low values of wall shear stress, while the opposite is true for the sweep events (Kim et al., 1987). The situation is the same for the MHD flows, but the strength of these events is reduced as indicated by the decrease of PD_{Q2} and PD_{Q4} for the extreme values of $\tau_w / \langle \tau_w \rangle_{Ef}$. Thus, fewer events correspond to the highest or lowest values of the wall shear stress and the maxima of PD_{Q2} and PD_{Q4} are increased and shifted to values $\tau_w / \langle \tau_w \rangle_{Ef} = 1$. The above is consistent with previous results showing that the fluid Reynolds shear stress and turbulence production are decreased by uniform magnetic fields (Lee and Choi, 2001; Krasnov et al., 2008).

Fig. 8b shows the probability density functions of the particle fluxes toward the wall PD_{Fin} and the channel central region PD_{Fout} with $\tau_w / \langle \tau_w \rangle_{Ef}$ for the hydrodynamic flow and representative MHD cases laden with particles of $S = 250$ and $\tau^+_p = 1$. Both PD_{Fin} and PD_{Fout} are calculated in the region of $5 \leqslant x^+_{2,0} \leqslant 15$. It is clear that, in the hydrodynamic case, PD_{Fin} and PD_{Fout} are well correlated to values of $\tau_w / \langle \tau_w \rangle_{Ef} > 1$ and $\tau_w / \langle \tau_w \rangle_{Ef} < 1$, respectively, which correspond to flow regions of sweep and ejection events (Marchioli and Soldati, 2002). This indicates that particles with small response times are transferred to the wall and the outer flow region mainly by strong organized fluids motions.

Such mechanisms can be considered universal and, thus, they are also observed in the presence of magnetic fields. Without the magnetic field, approximately 70% of the particles with $v'_2 < 0$ are found in flow regions corresponding to sweep events and about the same fraction of the particles with $v'_2 > 0$ are located in strong ejection events. These percentages of particles are slightly reduced by the magnetic field, while mixed trends are observed with respect to the effect of its orientation. The present study suggests that, in the MHD cases, the paths through which the particles are transferred close to the wall and away from it are equally effective as in the hydrodynamic flow. For all the cases, the total numbers of particles moving toward and away from the wall were almost equal, indicating that a statistically steady state was established. However, the total particle fluxes are reduced in the MHD flows and this is more apparent for a wall-normal magnetic field.

As already mentioned, in the hydrodynamic flows, high instantaneous particle concentrations coincide with regions of lower than the time-averaged streamwise fluid velocity in the near-wall region. Similar qualitative results are obtained in the MHD flows, but the preferential concentration of particles is affected by the suppression of the fluid velocity and vorticity fluctuations. This is demonstrated in Figs. 9a–d which show the instantaneous positions of particles with $S = 25$ and $\tau^+_p = 1$ located in a region of $x^+_{2,0} \leqslant 5$ at time $t^+ = 18{,}225$ for the hydrodynamic and MHD cases with streamwise ($N_1 = 0.1$), wall-normal ($N_2 = 0.006$), and spanwise ($N_3 = 0.025$) magnetic fields, respectively. Also shown in Fig. 9 are the contours of the streamwise fluid velocity fluctuations in the wall-parallel (x_1–x_3) plane at $x^+_{2,0} \leqslant 5$. Particles with $\tau^+_p = 1$ respond to a wide range of scales of fluid turbulence. Due to their

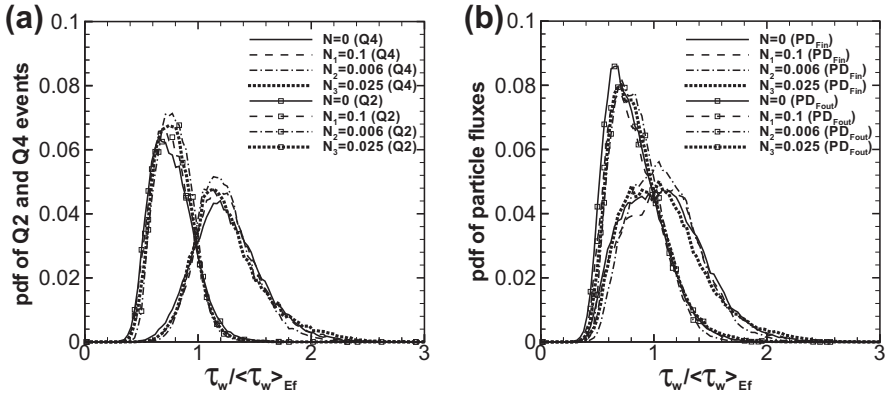

Fig. 8. Probability density functions (a) of sweep-*Q*2 and ejection-*Q*4 events and (b) of particle fluxes toward the wall (PD_{Fin}) and away from the wall (PD_{Fout}) in the region of $5 \leqslant x_{2,0}^{+} \leqslant 15$ for particles with $S = 250$ and $\tau_p^+ = 1$, without magnetic field ($N = 0$) and with streamwise ($N_1 = 0.1$), wall-normal ($N_2 = 0.006$), and spanwise ($N_3 = 0.025$) magnetic fields.

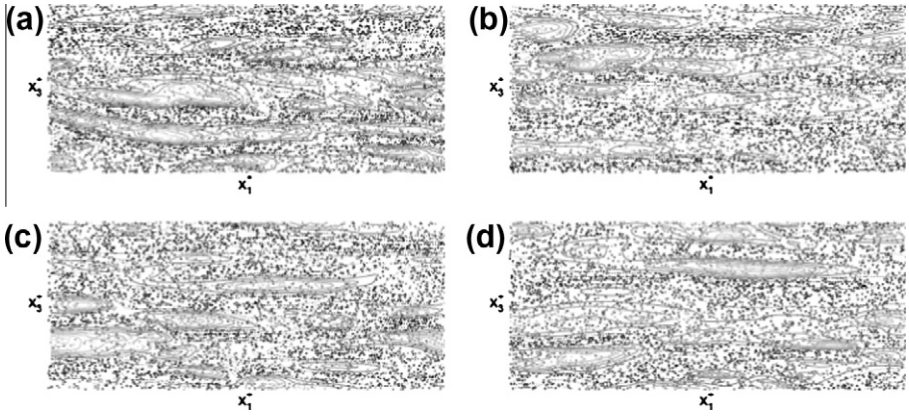

Fig. 9. Instantaneous distribution of streamwise velocity fluctuations at $x_{2,0}^{+} = 5$ and positions of particles with $\tau_p^+ = 1$ and $S = 25$ between $5 \leqslant x_{2,0}^{+} \leqslant 15$ at time $t^+ = 18{,}225$ for (a) $N = 0$, (b) $N_1 = 0.1$, (c) $N_2 = 0.006$, and (d) $N_3 = 0.025$. Empty spaces indicate low-speed streaks. The lighter dots denote high streamwise particle velocity fluctuations v_1', while the darker low v_1'.

inertia, once such particles are propelled in some direction by an intense vortical structure, they will continue their motion, increasing their distance from the event and resulting in regions void of particles. Fig. 9 confirms the tendency of particles to surpass regions of high streamwise velocities, tending to line up in low-speed streaks. Also shown, is the streamwise particle velocity fluctuations which exhibits an observable spatial correlation with themselves and with the underlying streamwise fluid velocity fluctuations. Similar results were obtained in the cases with particles of $S = 2.5$ or 250 and $\tau_p^+ = 1$, regardless of the magnetic field effect.

The pattern of alternative low- and high-speed streaks is related to the action of quasi-streamwise vortices near the wall (Kim et al., 1987). In the MHD cases, the size of the coherent structures is increased. The low-speed streaks are less intense and occupy larger volume relative to the hydrodynamic flow, as shown in Fig. 9. This was also verified by examining several Eulerian two-point fluid velocity correlations in the streamwise and spanwise directions. Thus, the total number of particles instantaneously concentrated in these particular flow regions is subsequently increased. In addition to their increased size, the strength of the vortical fluid events is reduced by the magnetic field (Lee and Choi, 2001; Krasnov et al., 2008; Dritselis and Vlachos, 2009), while a drastic depopulation of such events is also observed. Thus, the particle motion is less probable to be influenced by energetic turbulent structures, and the particles have a good chance of remaining in the quiescent low-speed streaks for longer times in the MHD cases.

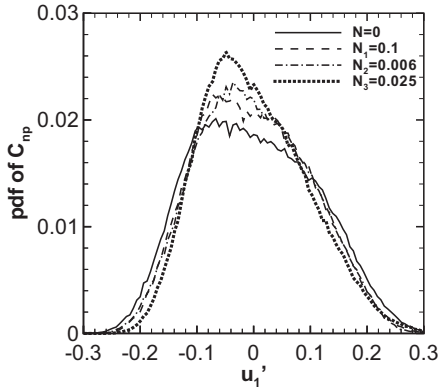

Fig. 10. Probability density function of the conditional particle number density for particles with $S = 250$ and $\tau_p^+ = 1$, without magnetic field ($N = 0$) and with streamwise ($N_1 = 0.1$), wall-normal ($N_2 = 0.006$), and spanwise ($N_3 = 0.025$) magnetic fields.

In order to quantify the above, the probability density function of the conditional particle number density PD_{cnp} in the region of $x_{2,0}^{+} \leqslant 5$ was calculated and it is shown in Fig. 10 as a function of the streamwise fluid velocity fluctuations. The values of PD_{cnp} were computed as follows: The instantaneous u_1 and mean U_1 streamwise fluid velocities were interpolated at the particle positions

and the corresponding fluctuation $u_1' = u_1 - U_1$ was determined. The number of particles associated with each value of u_1' was calculated and normalized by the population of particles within the volume of observation. Fig. 10 reveals that high particle number densities coincide with low streamwise fluid velocities as indicated by the bias between the negative and positive values of u_1' for all cases with $S = 250$ and $\tau_p^+ = 1$. This behaviour is consistent with previous findings of particle-laden turbulent channel flow (Pan and Banerjee, 1996; Marchioli and Soldati, 2002). In addition, this is observed regardless of the value of S and magnetic field orientation. In the MHD cases, the high magnitudes of u_1' are decreased and the fraction of particles associated with these values is reduced. Moreover, the maximum value of PD_{cnp} is increased and slightly shifted to more negative u_1' values, revealing a stronger tendency of particles to concentrate in regions with $u_1' < 0$, as compared to the hydrodynamic flow.

The interest so far was focused on addressing the magnetic field effect on the turbulent transport of particles rather than the effect of particle inertia, which has been widely investigated previously for hydrodynamic flows (McLaughlin, 1989; Young and Leeming, 1997; Rouson and Eaton, 2001; Marchioli et al., 2007). Thus, the discussion above was limited to particles with $\tau_p^+ = 1$. Qualitative similar results for the effect of magnetic field were obtained with increasing τ_p^+. However, with increasing inertia, the particle motion becomes less sensitive to the fluid turbulent fluctuations and it is little influenced by the flow changes observed in the MHD cases. Due to their low inertia, particles with small response times may act as tracers, exhibiting a uniform spatial distribution. On the other hand, particles with large response times attain random spatial distributions. This is because such particles move in almost straight lines inside the channel and they are not much influenced by the fluid motions or structures. Between these two extreme cases, the particles are affected by the underlying fluid motions, resulting in non-random spatial distributions. For example, the effect of the magnetic field on the near-wall spatial distribution of particles with $\tau_p^+ = 10$ is demonstrated in Fig. 11, which shows the instantaneous particle positions in a region of $x_{2,0}^+ \leqslant 5$ at $t^+ = 18{,}225$ for the hydrodynamic flow and the MHD case with $N_2 = 0.006$, respectively, in a similar manner as Fig. 9.

4.2.3. Particle deposition

The picture drawn so far is that, in the MHD cases, fewer particles are generally capable of reaching the channel wall. This is expected to have a considerable impact on the particle depositions rates, which is also investigated here by considering absorbing walls. A number of particles is now deposited at the walls and their total number remaining inside the channel is gradually reduced. In Fig. 12, the number of particles remaining inside the channel np_0–np_d normalized by its initial value np_0 is plotted as a function of the time from the release of the three particle sets with $\tau_p^+ = 1$ and $S = 2.5$, 25, and 250. It can be seen that after an initial transient, the slopes of the curves in Fig. 12 approach approximately asymptotic values as time increases, despite the particle accumulation in the near-wall region. This indicates that the number of deposited particles np_d per unit time remains nearly constant.

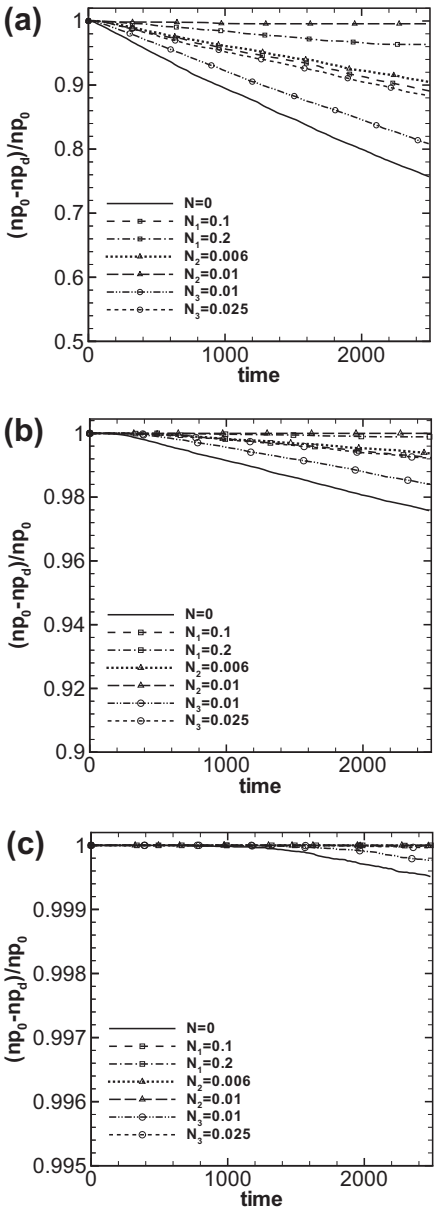

Fig. 12. Time histories of the particles remaining in the channel flow for particles with $\tau_p^+ = 1$ and $S = 2.5$ (a), $S = 25$ (b), and $S = 250$ (c). Without magnetic field ($N = 0$) and with streamwise ($N_1 = 0.1, 0.2$), wall-normal ($N_2 = 0.006, 0.01$), and spanwise ($N_3 = 0.01, 0.025$) magnetic fields.

The slopes of np_0–np_d are increased with increasing N or S, revealing indirectly a reduction of the particle deposition rate. As the lighter particles of $S = 2.5$ are transferred into the viscous sublayer, they cross smaller total distances before being deposited at the wall due to their larger diameter. This leads to faster rates of particle depletion, which is inhibited for the heavier particles.

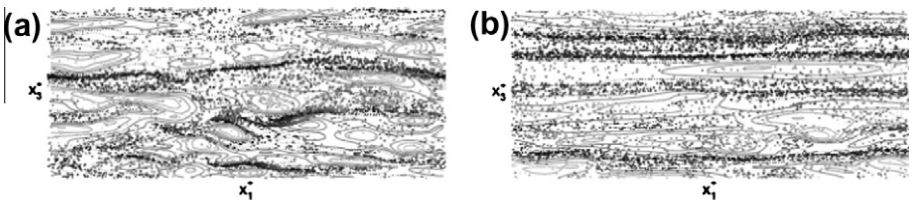

Fig. 11. Instantaneous distribution of streamwise velocity fluctuations at $x_{2,0}^+ = 5$ and positions of particles with $\tau_p^+ = 10$ between $5 \leqslant x_{2,0}^+ \leqslant 15$ at time $t^+ = 18{,}225$ for (a) $N = 0$ and (b) $N_2 = 0.006$. Empty spaces indicate low-speed streaks. The lighter dots denote high streamwise particle velocity fluctuations v_1', while the darker low v_1'.

The suppression of fluid turbulence and its structures by the magnetic field is reflected on the time history of the number of particles remaining in the channel flow. It is observed that the increase of the magnetic field results in slower particle depletion. The smaller reduction in np_0–np_d is observed for the magnetic field with spanwise orientation at $N_3 = 0.01$, which shows the smaller reduction in $u_{i,rms}$ among the MHD cases.

A proper measure for the particle deposition rate is the deposition velocity u_d^+ in wall units which is defined as (see, for example, Zhang and Ahmadi, 2000)

$$u_d^+ = J_p/(C_0 u_{\tau,0}), \tag{12}$$

where C_0 is the initial uniform particle concentration and J_p is the particle mass flux onto the deposition surface per unit time. In the present study, the particle deposition velocity is estimated as

$$u_d^+ = (np_d/t_d^+)/(np_0/y_0^+), \tag{13}$$

where the initial np_0 particles are located in a region of y_0^+ distance from the wall and t_d^+ is the time interval in which np_d particles are deposited. As discussed above, the calculation of u_d^+ was performed after the value of np_d/t_d^+ had become nearly constant.

Fig. 13 shows the deposition velocity u_d^+ as a function of N for several cases. It is generally observed that particle deposition is decreased with increasing N, while qualitative similar results are obtained for the three sets of particles with $\tau_p^+ = 1$ and $S = 2.5$, 25, and 250. However, the deposition rates are attenuated by increasing the particle–fluid density ratio; in some MHD cases, no particles were deposited. The largest reduction in u_d^+ is observed for the wall-normal and the smallest for the streamwise magnetic field.

The effect of the magnetic field on the deposition of particles with larger response times is illustrated in Fig. 14. Due to the faster depletion of these particles, the deposition velocity was calculated in the time interval between $t^+ = 1215$ and $t^+ = 1822$ after their release. The behaviour of particle deposition rates with increasing particle inertia in the absence of the magnetic field (McLaughlin, 1989; Zhang and Ahmadi, 2000; Marchioli et al., 2007) is well reproduced in the present simulations with a similar trend observed in the presence of the magnetic field. However, the deposition velocity u_d^+ is decreased for the range of τ_p^+ studied with the level of reduction being smaller for the heavier particles. Figs. 13 and 14 reveal that the particle deposition is more suppressed by a wall-normal magnetic field, while the reduction in u_d^+ is larger for a spanwise than a streamwise magnetic field.

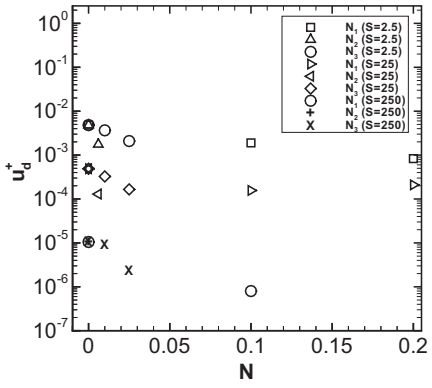

Fig. 13. Variation of particle deposition velocity for particles with $S = 2.5$, 25, and 250 and $\tau_p^+ = 1$, in the presence of streamwise ($N_1 = 0.1, 0.2$), wall-normal ($N_2 = 0.006, 0.01$), and spanwise ($N_3 = 0.01, 0.025$) magnetic fields.

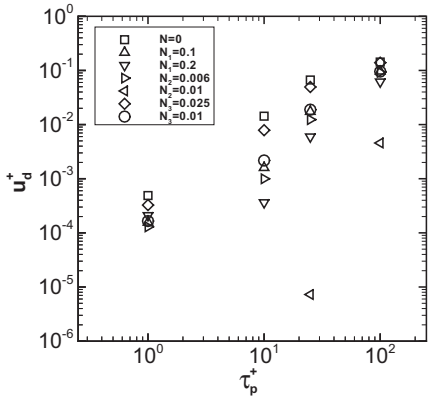

Fig. 14. Variation of particle deposition velocity with response time without magnetic field ($N = 0$) and with streamwise ($N_1 = 0.1, 0.2$), wall-normal ($N_2 = 0.006, 0.01$), and spanwise ($N_3 = 0.01, 0.025$) magnetic fields.

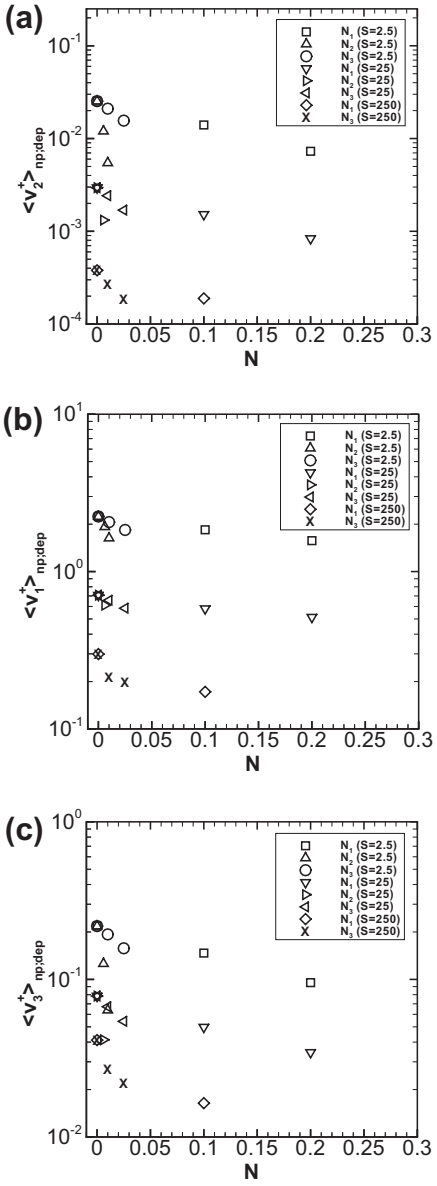

Fig. 15. Variation of the mean wall-impact particle velocity in the normal (a), streamwise (b), and spanwise (c) directions for $\tau_p^+ = 1$ with streamwise ($N_1 = 0.1, 0.2$), wall-normal ($N_2 = 0.006, 0.01$), and spanwise ($N_3 = 0.01, 0.025$) magnetic fields.

The wall-normal impinging velocity $v_{2,dep}$ of the deposited particles and their residence time t_R^+ inside a region of $x_{2,0}^+ < 5$ were also monitored. Based on these quantities, two populations were indentified, depending on whether a particle crossing the domain of observation performs a ballistic motion or not. In the case of ballistic motion, the particles were deposited due to their free-flight motion, while the deposition of all the other particles was considered to be due to turbulent diffusion. The deposition of small inertia particles is dominated by diffusion effects, while that of particles with large response times is mainly due to inertia. Particles with intermediate inertia are affected by the coherent structures and are deposited by either mechanism (McLaughlin, 1989; Zhang and Ahmadi, 2000; Marchioli et al., 2007). The present study indicates that the dominant deposition mechanism for all particle response times examined is not affected by the magnetic field. However, the wall-normal velocities of the small inertia particles deposited by turbulent diffusion are decreased in the MHD cases and, consequently, their residence times are increased. Similar results are obtained with increasing particle inertia, but the magnetic field effect is smaller in these cases.

The magnetic field effect on the mean wall-impact particle velocity $\langle v_2 \rangle_{np;dep}$ conditionally averaged over all depositing particles with $\tau_p^+ = 1$ as a function of N is shown in Fig. 15a in semi-log coordinates in order to magnify any differences produced by the orientation of the magnetic field. It should be pointed out that the knowledge of the wall-impact particle velocities is of great significance regarding wall erosion. Fig. 15a reveals that $\langle v_2 \rangle_{np;dep}$ is decreased with increasing S or N. Similar trends are observed for the streamwise $\langle v_1 \rangle_{np;dep}$ and spanwise $\langle v_3 \rangle_{np;dep}$ components of the mean wall-impact particle velocity shown in Figs. 15b and c, respectively. It can be seen that the values of $\langle v_3 \rangle_{np;dep}$ are larger than those of $\langle v_2 \rangle_{np;dep}$, and smaller than those of $\langle v_1 \rangle_{np;dep}$ Similar qualitative results for the effect of magnetic field on $\langle v_i \rangle_{np;dep}$ were obtained with increasing particle response time.

For all the cases, the particles lead the fluid near the walls, irrespective of the magnitude and the orientation of the magnetic field. The total drag force opposes the motion of particles during their crossing the viscous sublayer, causing them to gradually lose their momentum. The heavier particles remain for longer times in the near-wall region before they hit the wall and, consequently, their velocities are more reduced relative to the lighter particles. The overall magnetic damping effect on the fluid turbulence is also demonstrated indirectly by the variation of the mean wall-impact particle velocities shown in Fig. 15.

5. Conclusions

Direct numerical simulations were performed to assess the effect of the orientation and magnitude of a uniform magnetic field on the turbulent transport and deposition of uncharged, spherical particles in fully developed turbulent channel flows of electrically conducting fluids.

The particle dispersion in the wall-normal and spanwise directions is significantly damped by the magnetic field, while the opposite is observed in the streamwise direction, as indicated by the changes of the corresponding particle dispersion coefficients. The particles see fluid turbulent velocities that are correlated over longer times in the MHD than in the hydrodynamic flow.

The changes of fluid turbulence by the magnetic field are reflected on the dynamic behaviour of particles. The efficiency of the fluid structures responsible for particle dispersion is reduced in the MHD flows. Particle accumulation in the viscous sublayer is decreased and the magnetic field tends to smooth the non-uniformities of particle concentration near the wall. It was also shown that the mechanisms of turbophoretic drift and turbulent diffusion are less effective in the MHD flows. However, the particle fluxes toward the wall and the central region associated with intense organized fluid motions are not much influenced by the magnetic field.

The near-wall coherent vortices are enlarged and the low-speed streaks occupy larger volumes in MHD flows. Thus, an increased particle concentration is instantaneously found in regions of low streamwise fluid velocities. This is more apparent for increasing Hartmann number due to the transformation of the flow structures.

The particle deposition rates and the wall-impact velocities are decreased as a consequence of the overall damping of fluid turbulence by the magnetic field. With increasing inertia, the particle motion is less influenced by the local fluid turbulence and the changes generated by the magnetic field. The wall-normal magnetic field modifies more efficiently the turbulent structures and, thus, it has a stronger effect on the spatial distribution and deposition of particles. However, the dominant deposition mechanism is not affected by the magnetic field, but rather depends on particle inertia.

Acknowledgments

Financial support of CDD and IES from the Association EURATOM–Hellenic Republic is gratefully acknowledged. IES acknowledges travel support by the COST Action MP0806 "Particles in turbulence". The content of this paper is the sole responsibility of its authors and it does not necessarily represent the views of the European Commission or its services.

References

Armenio, V., Fiorotto, V., 2001. The importance of the forces acting on particles in turbulent flows. Phys. Fluids 13, 2437–2440.
Boeck, T., Krasnov, D., Zienicke, E., 2007. Numerical study of turbulent magnetohydrodynamic channel flow. J. Fluid Mech. 572, 179–188.
Braun, E.M., Mitchell, R.R., Nozawa, A., Wilson, D.R., Lu, F.K., 2008. Electromagnetic boundary layer flow control facility development using conductive particle seeding. In: 46th AIAA Aerospace Sciences Meeting and Exhibit, Reno, Nevada, USA, AIAA 2008-1396, pp. 1–12.
Caporaloni, M., Tampieri, F., Trombetti, F., Vittori, O., 1975. Transfer of particles in nonisotropic air turbulence. J. Atmos. Sci. 32, 565–568.
Choi, J.-I.I., Yeo, K., Lee, C., 2004. Lagrangian statistics in turbulent channel flow. Phys. Fluids 16, 779–793.
Davidson, P.A., 1997. The role of angular momentum in the magnetic damping of turbulence. J. Fluid Mech. 336, 123–150.
Davidson, P.A., 1999. Magnetohydrodynamics in materials processing. Annu. Rev. Fluid Mech. 31, 273–300.
Dritselis, C.D., Vlachos, N.S., 2009. On the effect of a transverse magnetic field on the coherent structures near the wall of a channel flow. In: Proceedings of Turbulence, Heat and Mass Transfer 6, Begell House, Inc., pp. 997–1000.
Eaton, J.K., Fessler, J.R., 1994. Preferential concentration of particles by turbulence. Int. J. Multiphase Flow 23, 169–209.
Fessler, J.R., Kulick, J.D., Eaton, J.K., 1994. Preferential concentration of heavy particles in a turbulent channel flow. Phys. Fluids 6, 3742–3749.
Homann, H., Bec, J., Fichtner, H., Grauer, R., 2009. Clustering of passive impurities in MHD turbulence. Phys. Plasmas 16, 082308.
Kaftori, D., Hetsroni, G., Banerjee, S., 1995. Particle behavior in the turbulent boundary layer. I. Motion, deposition, and entrainment. Phys. Fluids 7, 1095–1106.
Kakarantzas, S.C., Sarris, I.E., Grecos, A.P., Vlachos, N.S., 2009. Magnetohydrodynamic natural convection in a vertical cylindrical cavity with sinusoidal upper wall temperature. Int. J. Heat Mass Transfer 52, 250–259.
Kassinos, S.C., Knaepen, B., Carati, D., 2007. Passive scalar transport in MHD turbulence sheared in a rotating frame. Phys. Fluids 19, 015105.
Kassinos, S.C., Knaepen, B., Wray, A., 2006. Statistical measures of structural anisotropy in MHD turbulence subjected to mean shear and frame rotation. J. Turbul. 7 (26).
Kim, J., Moin, P., Moser, R., 1987. Turbulence statistics in fully developed channel flow at low Reynolds number. J. Fluid Mech. 177, 136–166.
Knaepen, B., Moreau, R., 2008. Magnetohydrodynamic turbulence at low magnetic Reynolds number. Annu. Rev. Fluid Mech. 40, 25–45.
Krasheninnikov, S.I., Smirnov, R.D., Pigarov, A.Yu., Soboleva, T.K., Mendis, D.A., 2010. Dust in fusion devices: the state of theory and modelling. J. Plasma Phys., doi:10.1017/S0022377809990560.
Krasnov, D., Zikanov, O., Schumacher, J., Boeck, T., 2008. Magnetohydrodynamic turbulence in a channel with spanwise magnetic field. Phys. Fluids 20, 095105.

Lee, D., Choi, H., 2001. Magnetohydrodynamic turbulent flow in a channel at low magnetic Reynolds number. J. Fluid Mech. 439, 367–394.
Leenov, D., Kolin, A., 1954. Theory of electromagnetophoresis. I Magnetohydrodynamic forces experienced by spherical and symmetrically oriented cylindrical particles. J. Chem. Phys. 22, 683–688.
Luo, J., Ushijima, T., Kitoh, O., Lu, Z., Liu, Y., 2007. Lagrangian dispersion in turbulent channel flow and its relationship to Eulerian statistics. Int. J. Heat Fluid Flow 28, 871–881.
Lykoudis, P.S., Brouillette, E.C., 1968. Magneto-fluid-mechanism channel flow. II. Theory. Phys. Fluids 10, 1002–1007.
Marchioli, C., Picciotto, M., Soldati, A., 2007. Influence of gravity and lift on particle velocity statistics and transfer rates in turbulent vertical channel flow. Int. J. Multiphase Flow 33, 227–251.
Marchioli, C., Soldati, A., 2002. Mechanisms for particle transfer and segregation in a turbulent boundary layer. J. Fluid Mech. 468, 283–315.
McLaughlin, J.B., 1989. Aerosol particle deposition in numerically simulated channel flow. Phys. Fluids A 1, 1211–1224.
Moffatt, H.K., Sellier, A., 2002. Migration of an insulating particle under the action of uniform ambient electric and magnetic fields. Part 1. General theory. J. Fluid Mech. 464, 279–286.
Moresco, P., Alboussière, T., 2004. Experimental study of the instability of the Hartmann layer. J. Fluid Mech. 504, 167–181.
Orlandi, P., 2000. Fluid Flow Phenomena: A Numerical Toolkit. Kluwer, Dordrecht.
Pan, Y., Banerjee, S., 1996. Numerical simulation of particle interaction with wall turbulence. Phys. Fluids 8, 2733–2755.
Pedinotti, S., Mariotti, G., Banerjee, S., 1992. Direct numerical simulation of particle behavior in the wall region of turbulent flow in horizontal channels. Int. J. Multiphase Flow 18, 927–941.
Rambaud, P., Tanière, A., Oesterlé, B., Buchlin, J.M., 2002. On the behavior of charged particles in the near wall region of a channel. Powder Technol. 125, 199–205.
Reeks, M.W., 1983. The transport of discrete particles in inhomogeneous turbulence. J. Atmos. Sci. 32, 729–739.
Rouson, D.W.I., Eaton, J.K., 2001. On the preferential concentration of solid particles in turbulent channel flow. J. Fluid Mech. 428, 149–169.
Rouson, D.W.I., Kassinos, S.C., Moulitsas, I., Sarris, I.E., Xu, X., 2008. Dispersed-phase structural anisotropy in homogeneous magnetohydrodynamic turbulence at low magnetic Reynolds number. Phys. Fluids 20, 025101.
Sarris, I.E., Iatridis, A.I., Dritselis, C.D., Vlachos, N.S., 2010. Magnetic field effect on the cooling of a low-Pr fluid in a vertical cylinder. Phys. Fluids 22, 017101.
Sarris, I.E., Kassinos, S.C., Carati, D., 2007. Large-eddy simulations of the turbulent Hartmann flow close to the transitional regime. Phys. Fluids 19, 085109.
Satake, S., Kunugi, T., Smolentsev, S., 2002. Direct numerical simulations of turbulent pipe flow in a transverse magnetic field. J. Turbul. 3 (20).
Sellier, A., 2003. Migration of an insulating particle under the action of uniform ambient electric and magnetic fields. Part 2. Boundary formulation and ellipsoidal particles. J. Fluid Mech. 488, 335–353.
Shatrov, V., Gerbeth, G., 2007. Magnetohydrodynamic drag reduction and its efficiency. Phys. Fluids 19, 035109.
Simonin, O., Deutsch, E., Minier, J.P., 1993. Eulerian prediction of the fluid-particle correlated motion in turbulent two-phase flows. Appl. Sci. Res. 51, 275–283.
Smirnov, R.D., Pigarov, A.Y., Rosenberg, M., Krasheninnikov, S.I., Mendis, D.A., 2007. Modelling of dynamics and transport of carbon dust particles in tokamaks. Plasma Phys. Control. Fusion 49, 347–371.
Squires, K.D., Eaton, J.K., 1991. Preferential concentration of particles by turbulence. Phys. Fluids A 3, 1169–1178.
Takahashi, K., Tanigushi, S., 2003. Electromagnetic separation of nonmetallic inclusion from liquid–metal by imposition of high frequency magnetic field. ISIJ Int. 43, 820–827.
Taylor, G.I., 1921. Diffusion by continuous movements. Proc. Lond. Math. Soc. 20, 196–211.
Wang, L.P., Maxey, M.R., 1993. Settling velocity and concentration distribution of heavy particles in homogeneous isotropic turbulence. J. Fluid Mech. 256, 27–68.
Wang, Q., Squires, K.D., Chen, M., McLaughlin, J.B., 1997. On the role of the lift force in turbulence simulation of particle deposition. Int. J. Multiphase Flow 23, 749–763.
Young, J., Leeming, A., 1997. A theory of particle deposition in turbulent pipe flow. J. Fluid Mech. 340, 129–159.
Zhang, H., Ahmadi, G., 2000. Aerosol particle transport and deposition in vertical and horizontal turbulent duct flows. J. Fluid Mech. 406, 55–80.
Zikanov, O., Thess, A., 1998. Direct numerical simulation of forced MHD turbulence at low magnetic Reynolds number. J. Fluid Mech. 358, 299–333.